Physical Wrapping of Reduced Graphene Oxide Sheets by Polyethylene Wax and Its Modification on the Mechanical Properties of Polyethylene

Zhenhu Cao,[1,2] Pingan Song,[3] Zhengping Fang,[1,2] Yuanyuan Xu,[1,2] Yan Zhang,[1] Zhenghong Guo[1]

[1]*Laboratory of Polymer Materials and Engineering, Ningbo Institute of Technology, Zhejiang University, Ningbo 315100, China*
[2]*MOE Key Laboratory of Macromolecular Synthesis and Functionalization, Institute of Polymer Composites, Zhejiang University, Hangzhou 310027, China*
[3]*Department of Materials, College of Engineering, Zhejiang Agriculture & Forest University, Hangzhou 300311, China*

Received 27 April 2011; accepted 16 January 2012
DOI 10.1002/app.36898
Published online in Wiley Online Library (wileyonlinelibrary.com).

ABSTRACT: A facile method to encapsulate the reduced graphene oxide (RGO) sheets physically with polyethylene (PE) wax was developed. The graphene oxide sheets were first wrapped with polyethylene wax, and reduced by hydrazine hydrate. The structure of the wrapped RGO was confirmed by means of Fourier transform infrared spectroscopy, X-ray diffraction (XRD), and Raman spectroscopy. The PE wax-wrapped RGO sheets were melt blended with PE to prepare PE/RGO nanocomposites. Transmission electron microscopy and XRD studies showed that this method could provide uniform dispersion of RGO sheets in the PE matrix. Scanning electron microscopy and Raman spectroscopy indicated that there was a strong interfacial interaction between the PE wax-wrapped RGO sheets and PE matrix. Addition of 1 wt % RGO sheets in PE matrix led to a 48% increment in the yield stress and 118% increment in the Young's modulus, respectively. However, the elongation at break decreased with increasing RGO sheets loading content. © 2012 Wiley Periodicals, Inc. J Appl Polym Sci 000: 000–000, 2012

Key words: polyethylene; graphene; polymer nanocomposites; mechanical properties

INTRODUCTION

Graphene, a thin layer material composed of sp^2 hybridized carbon atoms, was first isolated from graphite in 2004.[1,2] Up to now, attentions were focused on the application of graphene sheets in producing solar cells, hydrogen storages, sensors, and electronic devices as graphene sheets have super high electrical and thermal conductivity.[3–12] For the others, graphene sheets have a Young's modulus of 1 TPa and ultimate strength of 130 GPa.[13] High surface area (theoretical limit: 2630 m^2/g)[14] is another important advantage as reinforcements applied in nanocomposites compared with one dimensional carbon nanotubes[15,16] and two dimensional nanoclay.[17,18] So, polymer/graphene nanocomposites emerged as one of the most promising developments in the field of nanocomposites, endowing with significant advantages over conventional formulations.[19]

However, preparing polymer/graphene or graphene oxide (GO) nanocomposites requires that graphene sheets should be produced on a sufficient scale and dispersed very well in polymer matrix.[20] Many research works have been focused on grafting polar groups onto the surface of graphene or GO, and then preparing graphene-based polymer nanocomposites by blending the modified graphene or GO with polar matrices, such as poly(acrylonitrile), poly(vinyl alcohol) (PVA), polyurethane, and polymethyl methacrylate.[21] Liang et al.[22] prepared a nanocomposite with a 76% increase in tensile strength and a 62% improvement of Young's modulus are achieved by addition of only 0.7 wt % of GO in PVA. Zhao and coworkers[23] fabricated graphene/PVA nanocomposites via a facial aqueous solution blending and 150% improvement of tensile strength and a nearly 10 times increase of Young's modulus were achieved at a graphene loading of 1.8 vol %. However, up to now, few studies have been devoted to the reinforcement of nonpolar polymers with graphene or GO. Ruoff and coworker[24] yielded a uniform dispersion of the isocyanate functionalized graphene sheets in polystyrene (PS) solution to

Correspondence to: Z. Fang (zpfang@zju.edu.cn).
Contract grant sponsor: National Science Foundation of China; contract grant number: 51073140.
Contract grant sponsor: National Basic Research Program of China; contract grant number: 2011CB612307.

prepare PS/graphene nanocomposites. The PS/graphene nanocomposites exhibited an electrical percolation threshold of ~ 0.1 vol %, and a high conductivity of ~ 0.1 S/m at 1 vol % of graphene loading. Huang et al.[25] fabricated polypropylene (PP)/GO nanocomposites by *in situ* Ziegler–Natta polymerization. The PP/GO nanocomposites had a high electrical conductivity, 0.3 S/m when loading 4.9 wt % GO in PP matrix. Lin et al.[26] prepared polyethylene (PE)-*graft*-graphene hybrid material, which showed improved Young's modulus, yielding strength and tensile strength at very low loading of graphene. Kim et al.[27] reported graphene/polyethylene nanocomposites via solvent blending and melt compounding. Liner low-density polyethylene (LLDPE) was functionalized with —NH_2, —NHEt, —CN, and —NCO groups which enhanced the dispersion of thermally reduced graphene oxide (RGO) in LLDPE.

Although various methods have been applied in enhancing the dispersion of graphene or GO sheets in nonpolar matrix, these methods were limited to chemical modification of graphene or GO sheets. They needed strict reaction conditions and a large amount of organic agent. Herein, we present a facile route to prepare PE/RGO nanocomposites by melt blending PE with the RGO sheets which is physically wrapped with PE wax. The result showed that PE/RGO nanocomposites exhibited a significant enhancement in the mechanical properties at a low loading of RGO.

EXPERIMENTAL

Materials

Natural graphite powder (45 μm) was obtained from Alfa Aesar China (Tianjin, China). Concentrated sulfuric acid (H_2SO_4), hydrochloric acid (HCl), potassium permanganate ($KMnO_4$), sodium nitrate ($NaNO_3$), hydrogen peroxide (H_2O_2), and hydrazine hydrate (85%) were purchased from Shanghai Reagents Company, Shanghai, China. PE (LDPE: 2102TN26; Melt flow Index, 2.1–2.9; M_w, ca. 100,000; density, 0.920–0.922 g/m^3; and glass transition temperature, −78°C) was purchased from Sinopec Qilu Company, China. PE wax emulsion (solid content 40 wt %, solvent : water) was supplied from Aoda Chemical, Dongguan, China. All the materials were used directly without further purification.

Synthesis of graphite oxide

GO and RGO sheets were prepared by the route as shown in Figure 1. GO was synthesized according to the modified Hummers and Offeman's method.[28] Into a three-neck 500-mL flask, equipped with mechanical agitator, 10 g natural graphite powder and 5 g $NaNO_3$ were added in 400 mL concentrated H_2SO_4 at 0°C. Then, 36 g $KMnO_4$ was gradually added into the mixture under vigorous stirring at 20°C. Then the ice bath was removed and the mixture was kept stirring for 8 h when the temperature increased to room temperature. Afterwards, 800 mL deionized water was added into the mixture slowly, causing the mixture effervescence. After 15 min, the mixed solution of 30 mL 30% hydrogen peroxide and 2.5 L deionized warm water was added into the mixture with stirring. Upon treatment with the peroxide, the mixture was filtered while the filter cake was still warm. The filter cake was washed with dilute HCl aqueous solution three times and deionized water until the filter water near neutral. Finally, the resulting filter cake was dried under vacuum at 30°C for 3 days.

Fabrication of PE wax-wrapped reduced graphene oxide

To improve the dispersion of RGO sheets in PE matrix, PE wax emulsion was applied in wrapping RGO during the chemical reduction reaction in water. Into a one-neck 500-mL flask equipped with mechanical agitator, 1 g graphite oxide was dispersed in 500 mL 0.4 wt % PE wax emulsion by ultrasonic for 30 min. Then adding 0.2 mL hydrazine hydrate as the reducing agent into the mixture, and the mixture was heated to 95°C by oil bath with stirring for 6 h to finish the reduction process. The PE wax-wrapped RGO sheets were isolated by evaporating water in a desiccator. The average yield of RGO reduced from GO was 60 wt %.

Preparation of polyethylene/reduced graphene oxide sheets composites

PE and PE wax-wrapped RGO sheets were mixed in a Haake Minilab Rheomixer at a screw speed of 150 rpm for 12 min at 160°C. After mixing the samples, they were hot-pressed under 13 MPa for 10 min and then cooled down under the same pressure to get the sample sheets of suitable thickness. The composition containing 0.1, 0.5, 1.0, and 2.0 wt % RGO sheets and the resultant samples were designated as PE/*x*RGO-PE wax, where *x* denote the weight percentages of RGO. For comparison, the samples of pure PE and the same amount of PE wax were also prepared with the same procedure.

Characterization

Fourier transform infrared (FTIR) spectra of the GO powder, PE wax, and PE wax-wrapped RGO sheets were recorded on a Vector-22 FTIR Spectrometer using KBr pellet technology. The dispersion state of PE wax-wrapped RGO sheets in PE matrix were

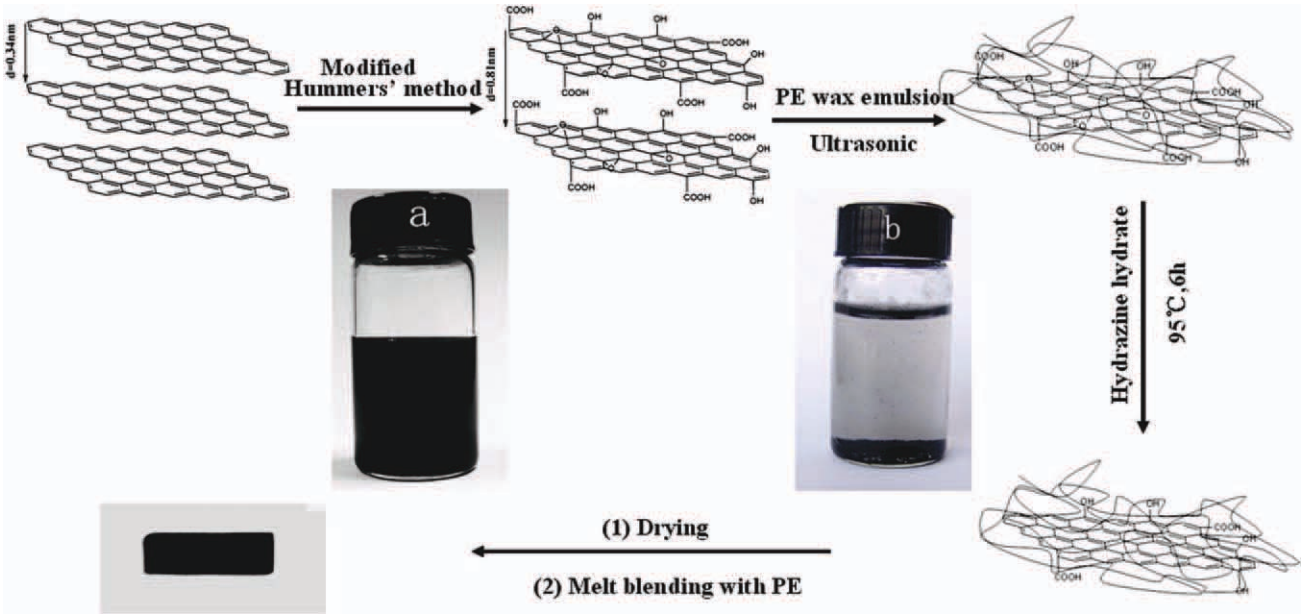

Figure 1 Schematic of synthetic route for preparation of graphite oxide (modified Hummers method), PE wax-wrapped GO sheets, and reduction by hydrazine hydrate solution and PE/RGO nanocomposites; and digital images of (a) PE wax-wrapped RGO sheets and (b) nonwrapped RGO in water (0.1% wt) after 7 days.

measured with transmission electron microscopy (TEM, JEM-1200EX) and X-ray diffraction (XRD, Rigaku X-ray generator, Cu Kα radiation).

Thermogravimetric (TG) and differential scanning calorimetric (DSC) analysis of composites were carried out under air atmosphere purge (120 mL/min) from room temperature to 600°C at a scanning rate of 20 °C/min by an integrative thermal analyzer instrument (TA-SDT Q600 instruments).

To measure the mechanical properties of the composites, the samples were cut to sheets with a 25 mm × 10 mm × 3.8 mm. The measurement was conducted with an XQ-1 tensile tester with a tensile rate of 20 mm/min and the gauge length of 25 mm. Dynamic mechanical properties were performed using a DMA242C dynamic mechanical analyzer. The tests were carried out in single-point bending mode at a vibration frequency of 2 Hz in a temperature range from −60 to 105°C at a heating rate of 5 °C/min under nitrogen. The morphology of fracture section and side-view of the PE/1.0 RGO-PE wax composite after tensile test were performed using a field emission scanning electron microscope (FEI sirion FESEM).

RESULTS AND DISCUSSION

Morphology of PE wax-wrapped RGO sheets

Atomic forced microscopy (AFM) and TEM images of GO sheets are shown in Figure 2. The AFM images showed single layer of GO sheets with an average thickness of about 0.75 nm [as shown in the Fig. 2(b) (2D) and (c) (3D) in the AFM image]. And typical lateral size of GO determined from Figure 2(a) (AFM image) and Figure 2(d) (TEM image) were in the range of several hundreds of nanometers to a few micrometers. The fact revealed that GO sheets were fully exfoliated.

Although GO sheets was very stable in aqueous solution,[29] RGO sheets can be easily re-stacking again by the effect of interlamination electrostatic force during the reduction process as shown in Figure 1(b). When RGO sheets were wrapped by PE wax, the suspensions showed long-term stability [7 days, as shown in Fig. 1(a)]. The strong interaction between PE wax and RGO sheets make the dispersion of the PE wax-wrapped RGO sheets stable in water.

Figure 3 shows the FTIR spectra of the GO, RGO sheets, and PE wax-wrapped RGO sheets. Noticeable absorptions of GO were located at 1723 cm^{-1} (carboxyl C=O stretching vibration), 1397 cm^{-1}(O—H deformation), and a broad band at 3000–3650 cm^{-1} which signified stretching vibration of hydroxyls and water absorption in the FTIR spectra [Fig. 3(a)].[30] For RGO sheets [Fig. 3(b)], absorption bands in 1723 cm^{-1} and 1397 cm^{-1} were disappeared and a wide absorption at 1100 cm^{-1} appeared. The result showed that GO was reduced by hydrazine hydrate. And PE wax-wrapped RGO [Fig. 3(c)] showed a strong absorption at 2857 cm^{-1} and 2922 cm^{-1} due to the C—H stretching in PE wax. It was indicated that PE wax was successfully wrapped with RGO sheets.

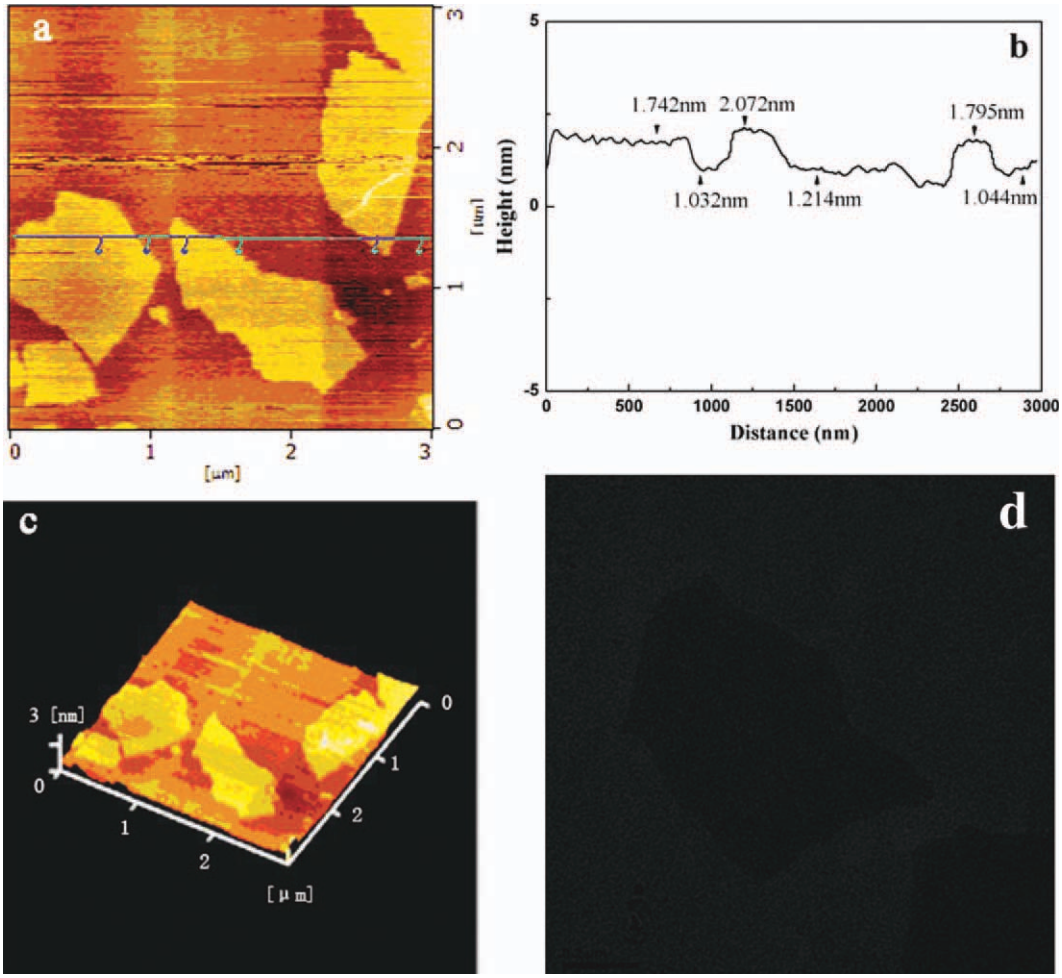

Figure 2 AFM and TEM images of GO. [Color figure can be viewed in the online issue, which is available at wileyonlinelibrary.com.]

XRD was used to evaluate the changes of interlayer distance of the nanosheets. As shown in Figure 4(a), pristine graphite exhibits a sharp diffraction peak at $2\theta = 26.4^\circ$, corresponding to the interlayer spacing of 0.34 nm. For GO [Fig. 4(b)], a strong reflection at about $2\theta = 10.7^\circ$ could be observed, corresponding to an interlayer spacing of 0.81 nm due to the intercalation by oxygen-containing groups and

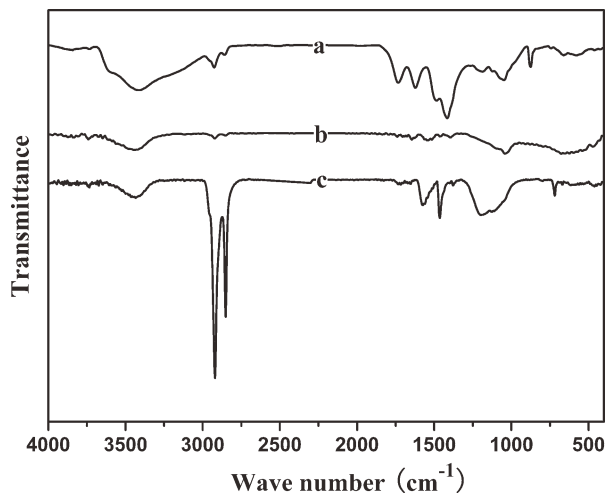

Figure 3 FTIR spectra of (a) graphite oxide, (b) RGO, and (c) PE wax-coated RGO nanosheets.

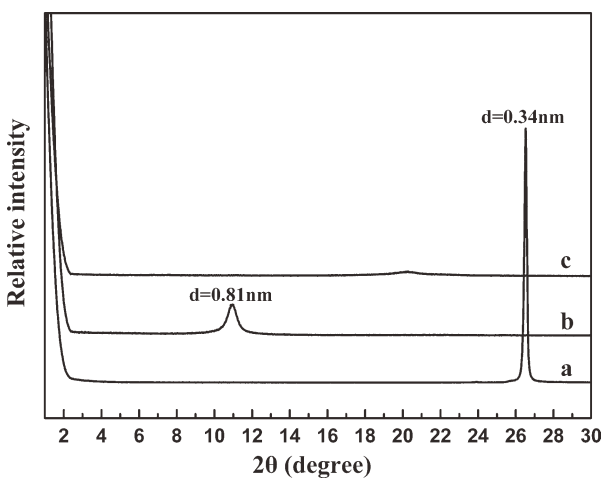

Figure 4 XRD pattern of (a) pristine graphite, (b) graphite oxide, and (c) PE wax-wrapped RGO sheets.

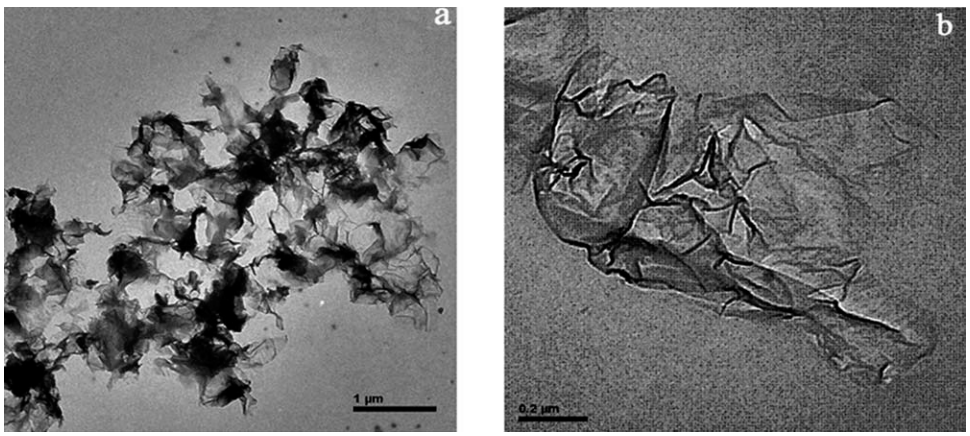

Figure 5 TEM images of PE wax-wrapped RGO sheets with different magnification.

moisture.[31] Whereas the XRD pattern of PE wax-wrapped RGO sheets [Fig. 4(c)] showed a broad trace and the characteristic peaks disappeared, inferring that PE wax-wrapped RGO sheets were exfoliated into a monolayer or few-layers which was significantly different from the pristine graphite and graphite oxide. It is concluded that PE wax played a very important role in balancing the electrostatic forces between the RGO sheets and retarding them restack again.

Figure 5 shows the TEM images of the morphology of PE wax-wrapped RGO. It can be seen from Figure 5(a) that the PE wax-wrapped RGO sheets has much more ripples than GO sheets as shown in Figure 2(d). And also, no reunion was observed. This result was in agreement with XRD patterns. In addition, the lateral size of PE wax-wrapped RGO was about 1 μm just as it can be seen from Figure 5(b).

Morphology of PE/RGO composites

The dispersion state of RGO sheets in the matrix were directly related with its effectiveness in improving mechanical, thermal, electrical, impermeability, and other properties. The morphology and the dispersion state of PE wax-wrapped RGO sheets in the PE matrix at different scales were studied by using a combination of TEM, Raman, and XRD.

TEM was used to evaluate the exfoliation and dispersion quality of RGO in the composites. Figure 6(a,b) shows TEM images of the PE/1.0 RGO-PE wax composites with different magnifications. RGO sheets displayed light black lines in PE matrix. It can be seen that RGO sheets dispersed very well in PE matrix and no large aggregated RGO sheets were observed.

Raman spectroscopy was widely used to obtain interfacial interaction between PE matrix and carbon-based materials.[32] Raman spectra of RGO sheets, PE and their composites obtained at an excitation wavelength of 532 nm were shown in Figure 7. In this part, the spectra of the RGO sheets displayed two characteristic peaks, the first at 1345 cm^{-1} attributed to the D band and derived from disordered graphite structure, the second located at 1586 cm^{-1} assigned the G band and associated with vibration of sp^2-hybridized

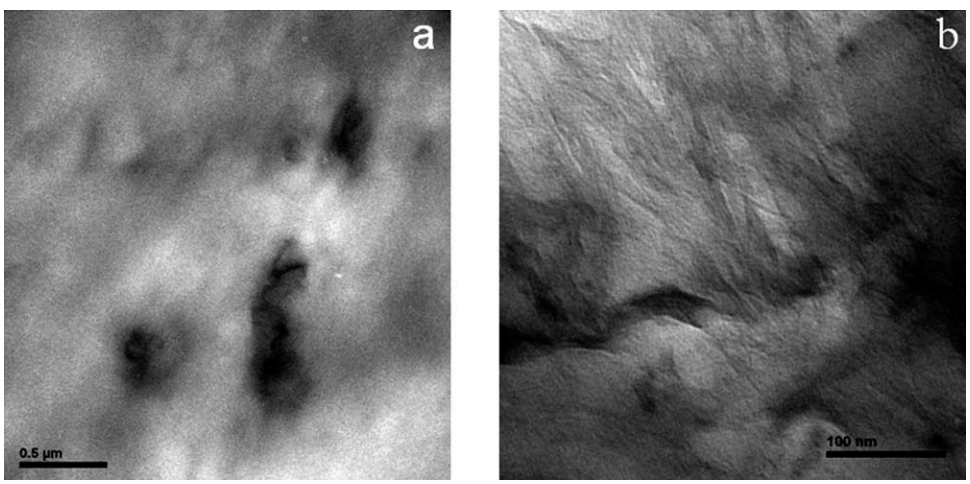

Figure 6 TEM image of PE/1.0RGO-PE wax composite with different magnification.

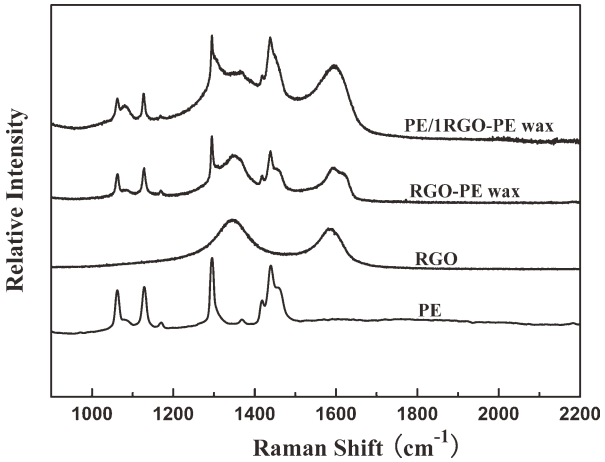

Figure 7 Raman spectra of PE, RGO, PE wax-wrapped RGO and PE/1.0RGO-PE wax composites.

graphitic domains. When RGO sheets were wrapped with PE wax, the G band peak was up-shifted by 4 cm^{-1}. Furthermore, loading 1 wt % RGO into PE matrix, the G band peak was up-shifted by 13 cm^{-1}. The shifting of G band peak to higher frequencies can be explained by the disentanglement of the RGO sheets and subsequent dispersion in the PE matrix as a consequence of the polymer chains penetrated into the PE wax-wrapped RGO sheets during melt blending. Similar up-shifting of G band has been reported for single-walled carbon nanotubes-reinforced PP.[33] The up-shifting of the D and G bands was also a consequence of strong compressive forces associated with PE chains on RGO sheets.

Further evidence for efficient dispersion and interconnectivity of RGO sheets in PE matrix was obtained from XRD patterns. As shown in Figure 8, there was no sharp peaks in about $2\theta = 26°$ which derived from the ordered restack of RGO sheets.

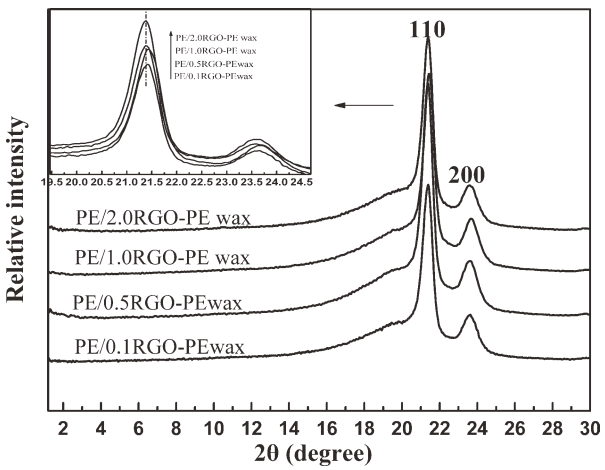

Figure 8 XRD patterns of PE/0.1RGO-PE wax, PE/0.5RGO-PEwax, PE/1.0RGO-PE wax, and PE/2.0RGO-PE wax composites.

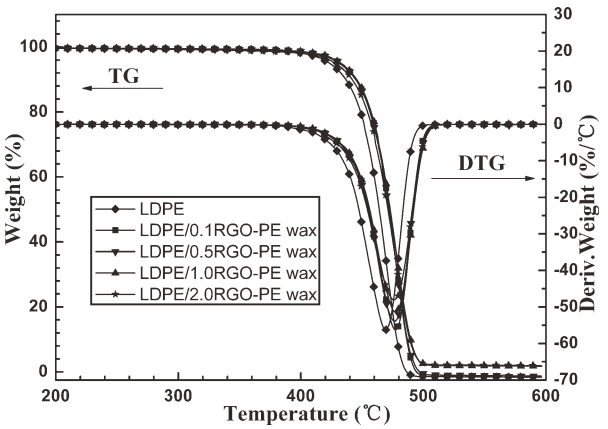

Figure 9 TG and DTG curves of LDPE, PE/0.1RGO-PE wax, PE/0.5RGO-PE wax, PE/1.0RGO-PE wax, and PE/2.0RGO-PE wax composites in N_2.

Furthermore, a little change in the peaks relating to the 110 and 200 reflections of PE with loading of RGO sheets indicated that the presence of RGO could, to some extent, affect the crystallization behavior of PE matrix.

Thermal analysis properties of PE/RGO composites

Thermal stability of the composites in nitrogen was investigated by thermogravimetric analysis (TGA). TGA curves and data of various samples are shown in Figure 9 and Table I, respectively. These results show that the degradation of PE starts from 422.5°C (T_{onset}) in N_2 and the maximum weight loss rate appears at 468.3°C (T_{max}). On incorporation of 0.1 wt % of RGO sheets in PE, the T_{onset}, and T_{max} was only $\sim$ 5°C and $\sim$ 9°C higher than pure PE, respectively. The temperature increase observed in the present study may arise from a similar barrier effect due to the hindered transport of degradation products caused by the numerous RGO sheets.[34,35]

Figure 10 and Table I show the differential scanning calorimetry (DSC) heating thermograms. The addition of RGO sheets increases the peak melting temperature of the PE/RGO composites. The addition of 0.1 wt % RGO sheets to PE slightly increases the peak melting temperature by 0.7–109.2°C. Further RGO sheets addition up to 2 wt % increase

TABLE I
Results of TG and DSC Analysis in N_2 at a Heating Rate of 20°C/min

Sample	T_{onset} (°C)	T_{max} (°C)	T_m (°C)	X_c (%)
PE	422.5	468.3	108.5	55.2 ± 1
PE/0.1 RGO-PE wax	427.7	477.2	109.2	56.7 ± 1
PE/0.5 RGO-PE wax	431.7	478.1	109.9	57.5 ± 1
PE/1.0 RGO-PE wax	432.4	478.5	111.3	58.8 ± 1
PE/2.0 RGO-PE wax	432.9	478.3	113.8	61.7 ± 1

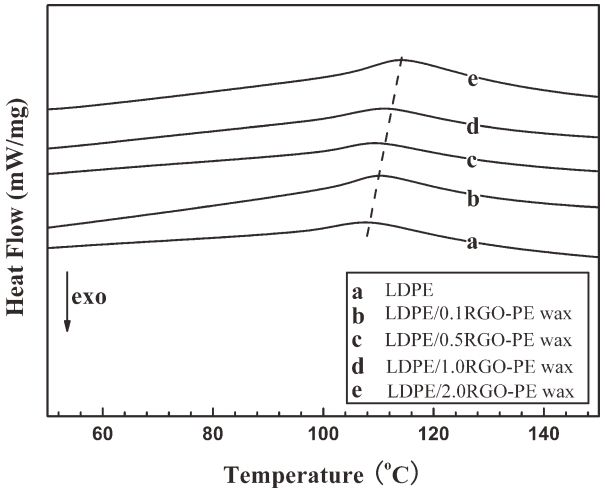

Figure 10 DSC curves of LDPE, PE/0.1RGO-PE wax, PE/0.5RGO-PE wax, PE/1.0RGO-PE wax, and PE/2.0RGO-PE wax composites in N_2.

the melting temperature to 113.8°C. In addition, in the composite with 2 wt % of RGO sheets the crystallinity reach to 61.7% and higher than pure PE 55.2%. The results indicated that RGO sheets may increase the degree of PE crystallinity,[36] and also it may enhance the mechanical properties of PE/RGO composites.

Mechanical properties of PE/RGO composites

RGO sheets have a larger surface area than other nanofillers such as carbon nanotubes (CNTs) and montmorillonite (MMT). Such a large surface area could induce an increased interaction between RGO sheets and polymer matrix. In polymer/RGO composites, if load can be effectively transferred from polymer matrix to RGO sheets, the strength and the modulus of the composites would be improved due to the fact that RGO sheets show higher modulus and strength than polymer matrix. The well-dispersed states of the fillers in polymer matrix and the good interfacial interaction between two components are key factors in order to prepare polymer composites with good mechanical properties.[14,23]

A representative stress–strain curve was illustrated in Figure 11 and the data of mechanical properties

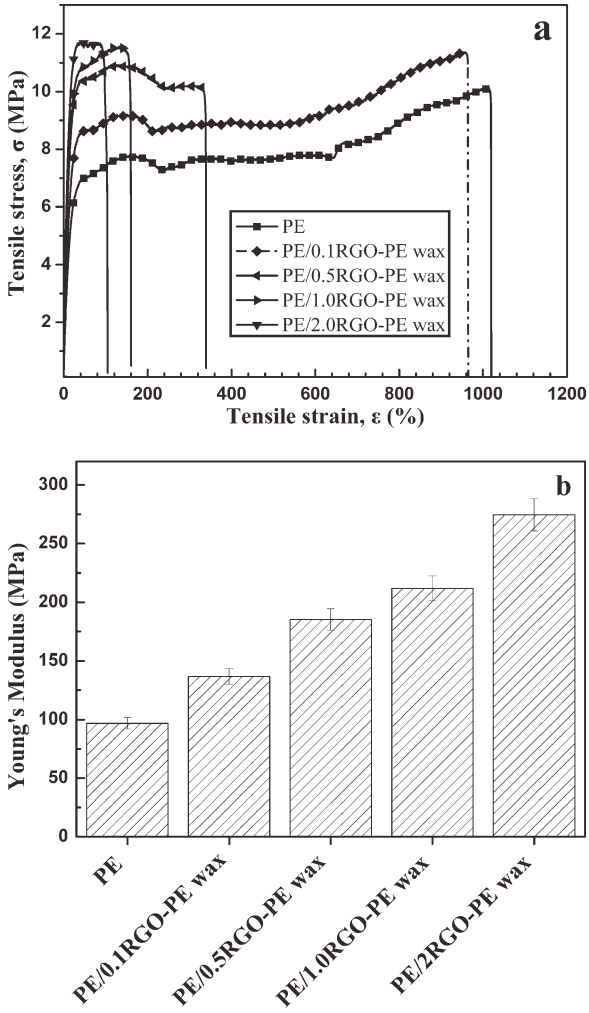

Figure 11 Tensile properties of the PE and its nanocomposites: (a) tensile stress–strain curves and (b) effect of RGO-PE wax content on the tensile modulus.

by tensile test are listed in Table II. As seen in Figure 11(a), pure PE matrix and PE/RGO composites with 0.1 wt % and 0.5 wt % RGO sheets show an elastic region followed by yielding that was accompanied by neck propagation. Loading 0.1 wt % and 0.5 wt % of RGO sheets in PE matrix increased the yield strength by 118% and 140%, respectively, compared with pure PE. However, the elongation of these samples decreased from 1015% to 961% and 334%,

TABLE II
Formulation and Mechanical Properties of PE and PE/RGO-PE Wax Nanocomposites

Sample	Young modulus (MPa)	Yield strength (MPa)	Breaking strength (MPa)	Strain at yield (%)	Strain at break (%)
PE	97 ± 3	7.8 ± 0.2	10.0 ± 0.2	156 ± 5	1015 ± 45
PE/0.1 RGO-PE wax	136 ± 6	9.2 ± 0.3	11.4 ± 0.2	138 ± 5	961 ± 39
PE/0.5 RGO-PE wax	185 ± 9	10.9 ± 0.2	10.4 ± 0.2	132 ± 7	334 ± 25
PE/1.0 RGO-PE wax	212 ± 12	11.6 ± 0.2	11.5 ± 0.2	134 ± 5	154 ± 10
PE/2.0 RGO-PE wax	275 ± 17	11.8 ± 0.2	11.5 ± 0.2	40 ± 3	93 ± 15

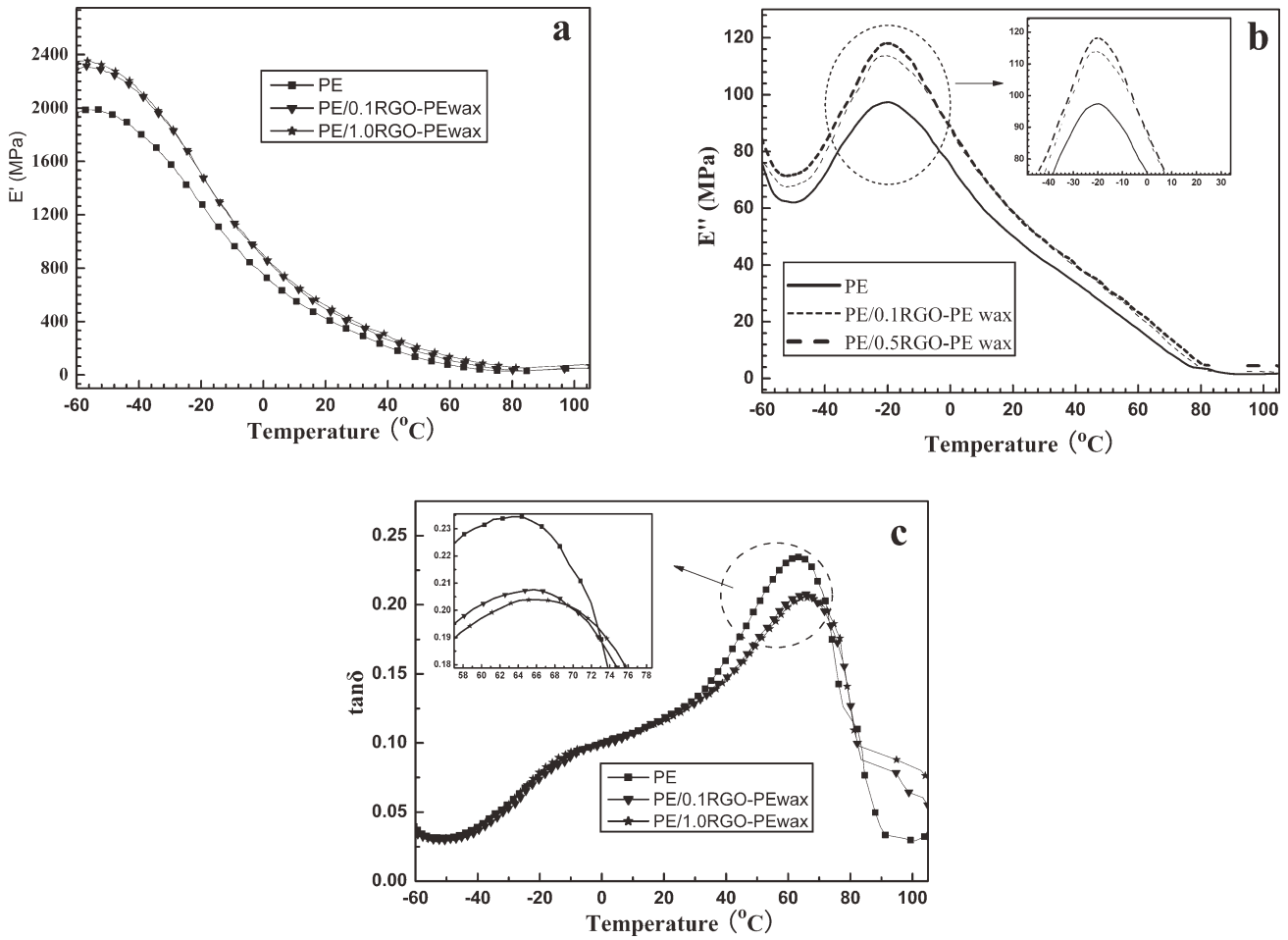

Figure 12 Variation of the storage modulus (E'), loss modulus (E'') and tan δ as a function of temperature, at 2 Hz, for PE/0.1RGO-PE wax and PE/1.0RGO-PE wax nanocomposites.

respectively. The above results indicated that the interfacial stress can be well transferred from PE matrix to RGO sheets. However, further addition of RGO sheets decreased the elongation but the yield strength and breaking strength remained higher than neat LDPE. When loading 2 wt % RGO sheets in PE matrix, the yield strength slightly increased to 11.8 MPa and the elongation decreased further to 93%. This might be due to the fact that loading RGO sheets in the LDPE matrix exceed the critical point[23] of the mechanical properties on the nano-sheets content, which results in agglomeration of

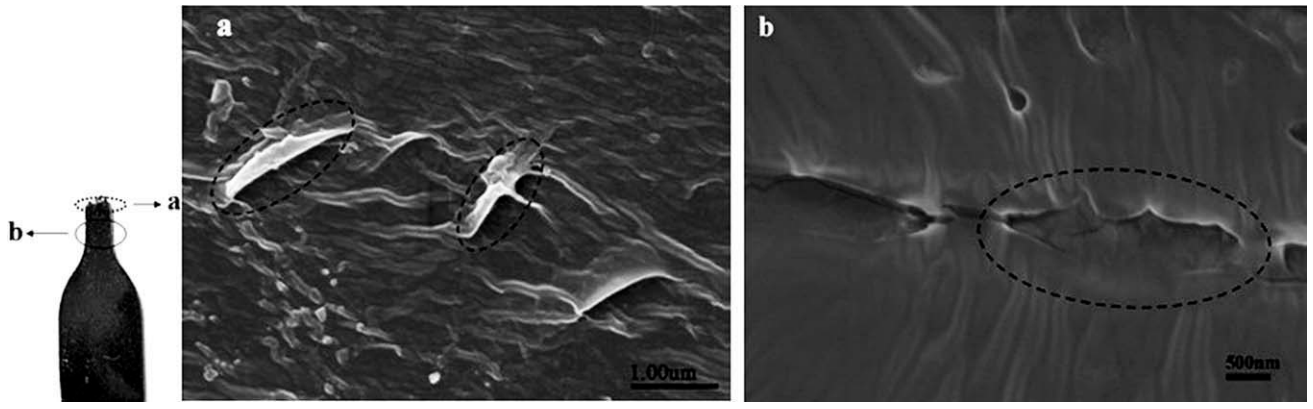

Figure 13 TEM images showing (a) the neck section and (b) the side-view of the fracture of the PE/1.0 PE wax-RGO composite after tensile test.

RGO sheets in LDPE matrix and decrease the elongation at break.[37] The Young's modulus (E) of the samples was determined from the slope of the initial elastic region. And as shown in Figure 11(b), the modulus of PE was about 97 MPa. Addition of 0.1 wt % RGO sheets to PE matrix increased the Young's modulus to 136 MPa. When loading 2.0 wt % RGO sheets in PE composites, the Young's modulus was enhanced about 2.8 times compared to PE. In short, the Young's modulus of PE/RGO-PE wax nanocomposites was much higher than pure PE.

The dynamic mechanical properties of PE and its nanocomposites between −60 °C and 105°C are shown in Figure 12. As expected, at −60°C E' was increased by about 17% on addition of 0.1 wt % RGO sheets compared with neat PE, and further increased by about 19% with 1.0 wt % RGO addition. Alone with temperature increase, the value of E' was decreased slowly. The dynamic loss modulus (E) was a measure of the energy absorbed due to a relaxation and thus was useful in clarifying the mechanisms of internal motions. As shown in Figure 12(b), loading 0.1 wt % and 1.0 wt % RGO sheets in PE matrix resulted in β relaxation peak which located at −20°C much more intense than pure PE. It was indicated that adding RGO sheets may increase the volume fraction of amorphous phase in PE matrix.[14] In addition, the damping factor (tan δ) curves of PE/RGO composites are shown in Figure 12(c). It can be seen that α peak relaxation increased from 62.6°C for pure PE to 65.4°C and 67.3°C, respectively. This result could be attributed to the fact that RGO sheets undergo deformation within the interfacial regions which were activated as a consequence of chain mobility in the crystals.

In order to detect the interfacial interaction between the PE matrix and PE wax-wrapped RGO sheets, the fracture surface of the PE composites was observed by scanning electronic microscope. Fracture surfaces of PE/1.0 RGO-PE wax composite are presented in Figure 13. The RGO sheets could be observed in Figure 13(a) which still embedded in the matrix and left protruding from the matrix. Yielding bent edges could be observed around the RGO sheets. Furthermore, the average particle size of the RGO sheets was the same as that of the original particles. It was interesting to note that in the side-view of the fracture of PE/1.0 RGO-PE wax composite [Fig. 13(b)], the most salient feature of the fracture surface was the propagation of the crack through the RGO sheets. At the same time, the matrix near the RGO sheets appeared multi deformation parallel lines perpendicular to the cracks. This result showed that the loading could be effectively transferred from PE matrix to RGO sheets in the composites.

CONCLUSIONS

GO sheets were wrapped with PE wax during chemical reduction. Then, nanocomposites with well-dispersed RGO sheets in PE matrix were successfully prepared through melt compounding PE with PE wax-wrapped RGO sheets. Significant enhancement in the mechanical properties of PE composites was observed. A 48% increase in tensile strength and 118% improvement in Young's modulus were achieved by adding 1.0 wt % RGO sheets PE matrix. The results indicated that the interfacial interaction between PE matrix and RGO sheets was strengthened through PE wax wrapping, so the efficient load transfer between the RGO sheets and the LDPE matrix. However, loading more RGO sheets in PE matrix lead to decrease in the elongation at break, which is an optimum loading content for improving the mechanical properties. Furthermore, the results indicate that physical wrapping RGO sheets provide a practical route towards low-cost bulk production. And it is a feasible approach for applying graphene nanosheets in various nonpolarity polymer matrices.

References

1. Novoselov, K. S.; Geim, A. K.; Morozov, S. V.; Jiang, D. Science 2004, 306, 666.
2. Novoselov, K. S.; Geim, A. K.; Morozov, S. V.; Jiang, D. Nature 2005, 438, 197.
3. Du, X.; Skachko, I.; Barker, A.; Andrei, E. Y. Nat Nanotechnol 2008, 3, 491.
4. Lee, C.; Wei, X.; Kysar, J. W.; Hone, J. Science 2008, 321, 385.
5. Balandin, A. A.; Ghosh, S.; Bao, W.; Calizo, I.; Teweldebrhan, D.; Miao, F.; Lau, C. N. Nano Lett 2008, 8, 902.
6. Novoselov, K. S.; Jiang, Z.; Zhang, Y.; Morozov, S. V.; Stromer, H. L.; Zeitler, U.; Maan, J. C.; Boebinger, G. S.; Kim, P.; Geim, A. K. Science 2007, 315, 1379.
7. Gomez, N. C.; Weitz, R. T.; Bittner, A. M.; Scolari, M.; Mews, A.; Burghard, M.; Kern, K. Nano Lett 2007, 7, 3499.
8. Castro, E. V.; Novoselov, K. S.; Morozov, S. V. Peres, N. M. R.; Santos, J. M. B. L. D.; Nilsson, J.; Guinea, F.; Geim, A. K.; Neto, A. H. C. Phys Rev Lett 2007, 99, 216802.
9. Kalaitzidou, K.; Fukushima, H.; Drzal, L. T. Composites: Part A 2007, 38, 1675.
10. Huang, X.; Zhou, X. Z.; Wu, S.; Wei, Y.; Qi, X.; Zhang, J.; Boey, F.; Zhang, H. Small 2010, 6, 513.
11. Stoller, M. D.; Park, S. J.; Zhu, Y. W.; An, J. H.; Ruoff, R. S. Nano Lett 2008, 8, 3498.
12. Frank, O.; Tsoukleri, G.; Parthenios, J.; Papagelis, K.; Riaz, I.; Jalil, R.; Novoselov, K.; Galiotis, C. ACS Nano 2010, 4, 5263.
13. Morcom, M.; Atkinson, K.; Simon, G. P. Polymer 2010, 51, 3540.
14. Kim, H.; Abdala, A. A.; Macosko, C.W. Macromolecules 2010, 43, 6515.
15. Coleman, J. N.; Khan, U.; Blau, W.; Gun'ko, Y. Carbon 2006, 44, 1624.
16. Moniruzzaman, M.; Winey, K. I. Macromolecules 2006, 39, 5194.
17. Giannelis, E. P. Adv Mater 1996, 8, 29.
18. Kumar, A. P.; Depan, D.; Tomer, N. S.; Singh, R. P. Prog Polym Sci 2009, 34, 479.

19. Qi, X.; Pu, K.; Li, H. Angew Chem Int Ed 2010, 49, 9426.
20. Jang, B. Z.; Zhamu, A. J Mater Sci 2008, 43, 5092.
21. Ramanathan, T.; Abdala, A. A.; Stankovich, S.; Dikin, D. A.; Herrera-Alonso, M.; Piner, R. D.; Adamson, D. H.; Schniepp, H. C.; Chen, X.; Ruoff, R. S.; Nguyen, S. T.; Aksay, I. A.; Prud'-Homme, R. K.; Brinson, L. C. Nat Nanotechnol 2008 3, 327.
22. Liang, J.; Huang, Y.; Zhang, L.; Wang, Y.; Ma, Y. F.; Guo, T. Y.; Chen, Y. S. Adv Funct Mater 2009, 19, 2297.
23. Zhao, X.; Zhang, Q.; Chen, D.; Lu, P. Macromolecules 2010, 43, 2357.
24. Stankovich, S.; Dikin, D. A.; Dommett, G. H. B.; Kohlhaas, K. M.; Zimney, E. J. ; Stach, E. A.; Piner, R. D.; Nguyen, S. T.; Ruoff, R. S. Nature 2006, 442, 282.
25. Huang, Y. J.; Qin, Y. W.; Zhou, Y.; Niu, H.; Yu, Z. Z.; Dong, J. Y. Chem Mater 2010, 22, 4096.
26. Lin, Y.; Jin, J.; Song, M. J Mater Chem 2011, 21, 3455.
27. Kim, H.; Kobayashi, S.; AbdurRahim, M. A. Polymer 2011, 52, 1837.
28. Hummers, W. S.; Offeman, R. E. J Am Chem Soc 1958, 80, 1339.
29. Paredes, J. I.; Villar-Rodil, S.; Martínez-Alonso, A.; Tascon, J. M. D. Langmuir 2008, 24, 10560.
30. Stankovich, S.; Piner, R. D.; Nguyen, S. T.; Ruoff, R. S. Carbon 2006, 44, 3342.
31. Titelman, G. I.; Gelman, V.; Bron, S.; Khalfin, R. L.; Cohen, Y.; Bianco, P. H.; Carbon 2005, 43, 641.
32. Tony, M.; Petra, P.; Peter, H. Polymer 2005, 46, 8222.
33. Valentini, L.; Biagiotti, J.; Kenny, J. M.; Santucc, S. Compos Sci Technol 2003, 63, 1149.
34. Barus, S.; Zanetti, M.; Bracco, P.; Musso, S.; Chiodoni, A.; Tagliaferro, A. Polym Degrad Stab 2010, 95, 756.
35. Kuila, T.; Saswata, B.; Hong, C.; Uddin, M. E.; Khanra, P.; Kim, N. H.; Lee, J. H. Carbon 2011, 49, 1033.
36. Fim, F. C.; Guterres, J. M.; Basso, N. R. S.; Galland, G. B. J Polym Sci Part A: Polym Chem 2010, 48, 692.
37. Khanna, Y. P.; Turi, E. A.; Taylor. T. J.; Vickory, V. V.; Abbott, R. F. Macromolecules 1985, 18, 1302.